INTERNATIONAL SOCIETY FOR
SOIL MECHANICS AND
GEOTECHNICAL ENGINEERING

SIMSG ISSMGE

This paper was downloaded from the Online Library of the International Society for Soil Mechanics and Geotechnical Engineering (ISSMGE). The library is available here:

https://www.issmge.org/publications/online-library

This is an open-access database that archives thousands of papers published under the Auspices of the ISSMGE.

The paper was published in the proceedings of the 11th International Conference on Physical Modelling in Geotechnics (ICPMG2026) and was edited by Ioannis Anastasopoulos. The conference was held from June 8th to June 12th 2026 in Zurich, Switzerland.

Proceedings of the 11th ICPMG 2026
11th International Conference on Physical Modelling in Geotechnics
8-12 June 2026, Zurich, Switzerland
© 2026 the Authors

Effect of Tip Angle on Cone Penetration Resistance: Insight from Model Test and DEM Analysis

R. Nakamura
Port and Airport Research Institute, Kanagawa, Japan, nakamura-r@p.mpat.go.jp,
NEWJEC Inc., Osaka, Japan, nakamurary@newjec.co.jp

M. Otsubo, R. Sukhumkitcharoen, A. Kondo, I. Sato and O. Kurihara
Port and Airport Research Institute, Kanagawa, Japan,
otsubo-m@p.mpat.go.jp, sukhumkitcharoen@p.mpat.go.jp, kondoh-a@p.mpat.go.jp,
satoh-i-p@p.mpat.go.jp, kurihara-oo@p.mpat.go.jp

H. Takahashi
Tokyo University of Marine Science and Technology, Tokyo, Japan, takahashi-h@kaiyodai.ac.jp

ABSTRACT: The cone penetration test (CPT) is widely used to evaluate the mechanical properties of in-situ soil, where the measured cone tip resistance q_c reflects soil strength. Although cone geometry is standardized, variations in cone tip angle significantly influence the stress field during penetration, leading to systematic differences in measured resistance. However, the combined effects of cone tip angle and stress level are not yet fully quantified. This study investigates the influence of cone tip angle on q_c of sandy soil through physical model experiments and discrete element method (DEM) simulations. CPTs were conducted in a $1g$ model test using cones with different tip angles. The experimental results show that q_c increases monotonically with increasing effective vertical stress for all cone geometries. At a given stress level, larger tip angles lead to higher q_c, and this dependency becomes more pronounced under higher effective stress conditions. DEM simulations qualitatively capture these trends and provide micromechanical insights into the "shape effect" of the cone. The analysis reveals that blunter cones (larger tip angles) intensify vertical particle movement and contact pressure concentration near the cone shoulder, and vice versa. These findings demonstrate that q_c is governed by the interaction between cone geometry and the localized stress field, providing a fundamental basis for interpreting CPT data when compared with other types of penetration tests with various cone configurations.

1 INTRODUCTION

The cone penetration test (CPT) is one of the most widely used in-situ tests for evaluating the mechanical properties of soils in both onshore and offshore sites. The measured cone tip resistance q_c reflects the shear strength of the ground, and plays a key role in bearing capacity evaluation and soil classification. Although CPT cone geometry is standardized, examining tip-angle effects remains necessary to interpret stress redistribution during penetration and to enable meaningful comparison with other penetration tests employing different cone configurations.

Experimental investigations into this shape effect have a long history. Nowatzki and Karafiath (1972) demonstrated that varying cone angles mobilize different stress concentration in soil. Durgunoglu and Mitchell (1973) systematically examined cone angles ranging from 30° to 180°, clarifying their influence on both resistance and failure zones, and proposed a combined plane and radial shear mechanism. More recently, Iikawa and Katsuragi (2024) used a 2D visualization test to show that greater tip angles intensify particle confinement and dilative flow, leading to a nonlinear increase in resistance.

From a theoretical standpoint, Baligh (1985) introduced the strain path method for large deformation analysis of cone penetration, and Yu and Mitchell (1998) reviewed major analytical approaches including bearing capacity, cavity expansion, and finite element methods, emphasizing that combined theoretical frameworks are necessary to capture the effects of tip angle, friction, and stress path.

Recent studies have also focused on the influence of grain size, relative density D_r , and stress conditions on CPT resistance. Laboratory and calibration-chamber experiments (Ahmadi, 2009; Zhuang and Yu, 2018) have revealed clear size and density effects, while Ahmadi and Karambakhsh (2010) proposed an empirical relationship showing strong dependence of q_c on D_r and effective horizontal stress σ'_h.

Recent DEM studies have also examined the influence of tip geometry in the context of CPT-based interpretations for rotary-installed piles. For example, Sharif et al. (2021) systematically investigated the effect of tip angle on installation force and torque, and proposed a modified CPT-based prediction framework. However, in their study, q_c was evaluated with reference to the cone tip rather than the cone shoulder, and the analysis focused primarily on resultant forces and averaged stress components. As such, the spatial distribution of contact pressure acting on the cone surface and its relationship to the stress reference level commonly adopted in CPT interpretation were not explicitly addressed.

Moreover, a systematic investigation by combining physical model tests and DEM simulations remain limited. Therefore, this study employs DEM to investigate in detail the effects of cone tip angle on q_c and contact stress in sand.

2 METHODOLOGY

The objective of this study is to investigate the influence of cone tip angle on q_c of sand during CPT. To achieve this goal, a three-stage research framework was designed, combining physical model tests and numerical analyses using DEM.

An overview of the research flow is illustrated in Figure 1 and summarized briefly as below.

Stage 1: Physical model test

Small-scale CPT were conducted in saturated sand to experimentally capture the effect of cone tip angle on q_c . By varying the tip angle while maintaining other parameters constant, the fundamental relationship between cone geometry and measured q_c was identified.

Stage 2: DEM simulation

The DEM results were qualitatively compared with the experimental data to evaluate the consistency of the numerical model in capturing the trends of macroscopic penetration resistance and the deformation mechanism of the sand. This qualitative agreement ensures that the DEM model can be used to explore parameter variations beyond the experimental range.

Stage 3: Micromechanical investigation

After model validation, a systematic parametric study was performed using DEM. The cone tip angle was varied to examine their combined influence on q_c and local stress transfer mechanisms.

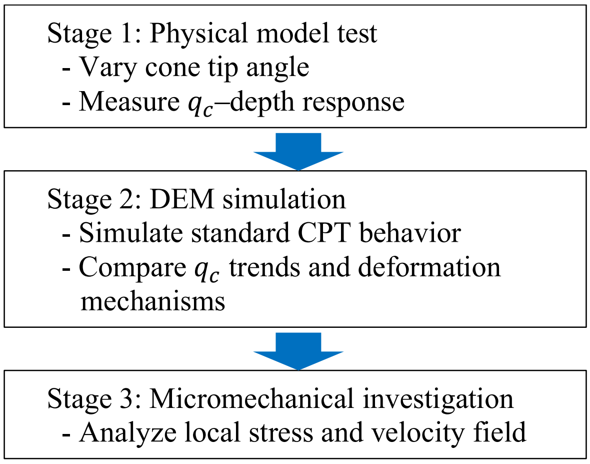

Figure 1 Research flow of the study

3 PHYSICAL MODELLING

3.1 Test conditions

The penetration tests were conducted at $1g$ in the same large container filled with saturated sandy soil, which had been previously subjected to centrifugal acceleration at $50g$ to induce overconsolidation and ensure soil homogeneity. The penetration positions in each test case were arranged to satisfy the condition of a distance-to-cone diameter ratio $S/D \geq 20$ from the sidewall, in order to sufficiently minimize boundary effects (Bolton et al., 1999; Zhuang and Yu, 2018). In addition, the spacing between adjacent penetration tests was maintained at not less than 7.5 times the cone diameter. This spacing was separately confirmed to have a negligible influence on q_c.

The test material was uniform saturated sand, as summarized in Table 1. The specimen was prepared by the air pluviation method, and D_r approximately 53.1 % was achieved. After deposition, the surface of the sand was leveled.

One-third-scale cones based on the standard CPT diameter of 35.7 mm, with different tip angles, were fabricated from stainless steel. The cone diameter was 12 mm, and seven tip angles were tested: 30°, 45°, 60°, 90°, 120°, 150° and 180°. Each cone was equipped with a load cell to measure the vertical penetration force. As shown in Figure 2, only the vertical resistance acting below the cone shoulder was measured, and frictional resistance mobilized along the sleeve was not included in the recorded force. The penetration was performed vertically at a constant rate of about 30.7 mm/min. The penetration depth was defined as the distance from the initial ground surface to the cone shoulder. q_c was then calculated by dividing the measured vertical load F_z by the projected cone tip area A_{tip}.

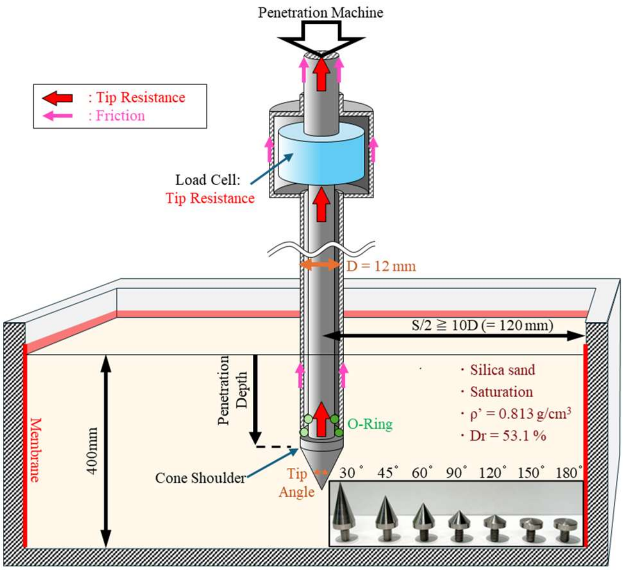

Figure 2 Schematic illustration of the model cone penetration test setup (not to scale)

Table 1. Sand properties

Properties	Contents
Soil type	Silica sand
Median grain size $\boldsymbol{D_{50}}$	0.16 mm
Specific gravity $\boldsymbol{G_s}$	2.64
Maximum void ratio $\boldsymbol{e_{max}}$	1.275
Minimum void ratio $\boldsymbol{e_{min}}$	0.789
Relative density $\boldsymbol{D_r}$	53.1 %
Effective unit weight $\boldsymbol{\gamma'}$	7.97 kN/m³

3.2 Experimental results

In the present analysis, effective vertical stress σ'_v was evaluated at the cone shoulder depth (Figure 2) and q_c was calculated by subtracting the buoyant force acting on the cone and the rod.

As shown in Figure 3, for all cone tip angles tested, q_c increases monotonically with increasing σ'_v. This trend is consistently observed over the entire stress range considered, indicating a clear stress dependency of the measured q_c regardless of cone geometry.

Figure 4 shows that, at a given σ'_v level, q_c systematically increases with increasing cone tip angle. This angle dependency is observed at all examined stress levels, and the difference in q_c between cones with different tip angles becomes more pronounced as σ'_v increases. The values of q_c were observed to be 100 to 200 times σ'_v.

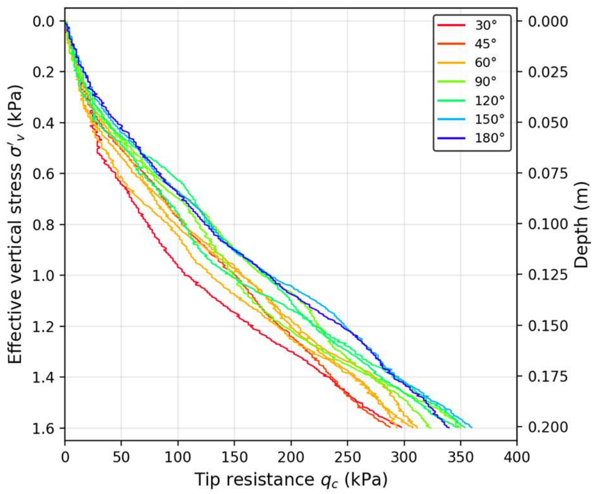

Figure 3 Experimental relationship between q_c and σ'_v evaluated at the cone shoulder

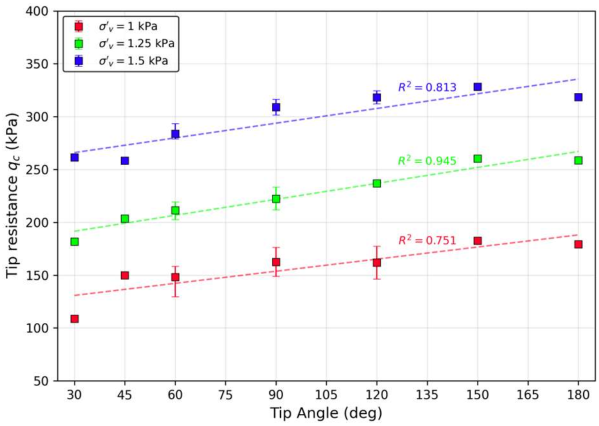

Figure 4 Experimental dependence of mean q_c on cone tip angle at different σ'_v levels (Error bars indicate experimental ranges).

3.3 Discussions

The results demonstrate that q_c is strongly dependent on both σ'_v and cone tip geometry. In particular, a monotonic increase in q_c with increasing σ'_v is consistently observed for all cone tip angles investigated.

Evaluating σ'_v at the cone shoulder depth enables a stable and systematic organization of the experimental results obtained with different cone tip angles. This approach is physically consistent, as the soil deformation zone during cone penetration is not confined to the immediate vicinity of the cone tip but extends to the shoulder region. This interpretation is based on experimental observations and involves a degree of inference.

Furthermore, at a given σ'_v level, cones with larger tip angles exhibit higher q_c, and this angle effect becomes more pronounced as σ'_v increases. These results suggest that the influence of cone geometry on q_c is enhanced under higher confinement. However, the detailed micromechanical mechanisms responsible for this behavior cannot be identified from the experimental results alone.

Overall, the physical model experiments clearly capture both stress-dependent and geometry-dependent characteristics of q_c.

4 NUMERICAL MODELING

4.1 Analysis conditions

To further investigate the underlying mechanisms governing these experimental trends, DEM simulations are conducted. A simplified Hertz–Mindlin contact model (Mindlin and Deresiewicz, 1953) was employed in the Large-scale Atomic/Molecular Massively Parallel Simulator (LAMMPS; Plimpton, 1995) to simulate the interaction between granular soil and the cone-tipped pile.

The soil chamber (Figure 5a) was modeled as a quarter-sector of a rigid cylindrical container with a radius of 0.4 m. To optimize computational efficiency while maintaining high resolution near the penetration zone, the assembly was created using the particle refinement method (PRM) (Mcdowell et al., 2012; Sharif et al., 2021). The assembly contained a total of 60,989 particles. To reduce computational cost, a radially increasing particle size distribution was implemented across seven concentric layers. The outer radius of each successive layer was set to 1.42 times the radius of the adjacent inner layer. Correspondingly, D_{50} in each layer was scaled by a factor of 1.3 relative to the inner layer, ranging from 3.5 mm in the innermost penetration zone to 17 mm at the outermost boundary. The layer thickness t_L was determined to ensure a sufficient t_L/D_{50} ratio in each zone for representative stress transmission. Detailed parameters for each layer are summarized in Table 2.

The particle density was set to 2.65 g/cm³. The target void ratio of 0.681 ($D_r = 50$ %) was achieved through a gravitational deposition process. Initially, particles were randomly generated within the chamber volume. During the deposition stage, the interparticle friction coefficient was systematically adjusted within the range of 0.0 to 0.35. By reducing the friction during pluviation, a denser packing was obtained, whereas higher friction led to a looser structure. Once the target void ratio was reached and the kinetic energy of the assembly dissipated, the friction coefficient was reset to the final analysis value of 0.35 to ensure consistency during the penetration simulation.

The pile was modeled as a rigid assembly consisting of four sections (b), with a pile diameter d_c of 35.7 mm and a fixed cone apex angle of 30–180°. A constant downward penetration velocity v_{cone} of 0.02 m/s in Z-direction was applied, same as the CPT standard. It was also checked that the applied velocity resulted in negligible inertial effects. The inertial number expresses the ratio of inertial forces to confining forces and is computed (Janda and Ooi, 2016; Ciantia et al., 2019; Lei et al., 2024) as:

$$I = \dot{\gamma} D_{50} \sqrt{\rho/P} \quad (1)$$

$$\dot{\gamma} = v_{cone}/L_p \quad (2)$$

where $\dot{\gamma}$ is the shear strain rate, D_{50} is the median diameter of the central layer particles, ρ is the particle density, P is the confining pressure and L_p is the width of the plastic zone formed under the tip. Assuming that, $L_p = 3d_c$ the precedent formulas may be employed to compute the maximum shear strain rates and penetration velocities compatible with a particular value of the inertial number. Janda and Ooi (2016) suggested that values of $I \approx 0.01$ are enough to ensure quasi-static conditions. At $P = 0.5$

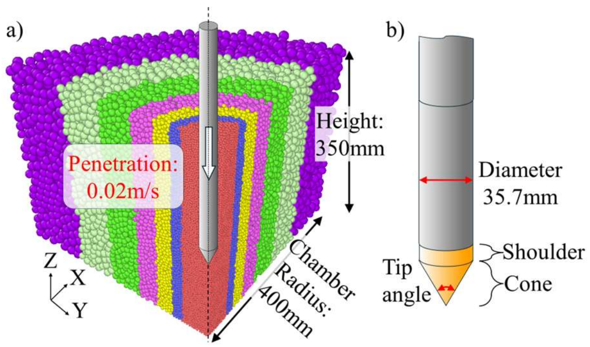

Figure 5 Schematic illustration of the CPT model in DEM simulations: (a) soil chamber and (b) pile geometry.

Table 2 Configuration of the radially graded particle layers in DEM.

Layer	Outer Radius $\boldsymbol{R}$ (mm)	Layer thickness $\boldsymbol{t_L}$ (mm)	$\boldsymbol{D_{50}}$ (mm)	$\boldsymbol{t_L/D_{50}}$
1	50	50	3.5	14.29
2	70	20	4.6	4.35
3	100	30	6.0	5.00
4	140	40	7.7	5.19
5	200	60	10.0	6.00
6	280	80	13.0	6.15
7	400	120	17.0	7.06

kPa, 1.0 kPa and 2.0 kPa, I were found to be 0.0015, 0.0011 and 0.0008, respectively. These values are well below the critical threshold of 0.01, confirming that the penetration process remains within the quasi-static regime.

The interparticle friction coefficients between particle–particle, particle–pile, particle–exterior wall and particle–XY boundary wall contacts were set to 0.35, 0.35, 0.0 and 0.1, respectively.

While the physical experiments were conducted under saturated conditions, the DEM simulations were performed in a dry environment using the effective stress principle. Since the penetration rate was sufficiently low to ensure drained conditions in the sand, the mechanical behavior is primarily governed by grain-to-grain contact forces. Therefore, the DEM model focuses on capturing the influence of cone geometry on the soil skeleton's stress distribution and particle kinematics, providing a qualitative basis for interpreting the experimental results.

4.2 Numerical results

The results of the DEM simulations are presented in terms of the relationships between q_c, σ'_v, and the cone tip angle, as well as the local distributions of contact pressure and particle motion around the cone.

Figure 6 shows the relationship between q_c and σ'_v, evaluated at the cone shoulder depth for different cone tip angles, after applying moving-average smoothing with a ± 0.25 kPa window. For all cone geometries considered, q_c increases monotonically with increasing σ'_v. This trend is consistently observed over the entire stress range investigated, indicating a clear stress dependency of the numerically obtained q_c.

The dependence of q_c on cone tip angle is summarized in Figure 7, where mean values of q_c are evaluated over selected effective stress ranges. At a given σ'_v level, q_c systematically increases with increasing cone tip angle. This angle dependency is consistently reproduced across all examined stress levels, and the difference in q_c between cones with different tip angles becomes more pronounced at higher effective stress levels. The values of q_c were observed to be 20 to 30 times σ'_v.

Local mechanical responses obtained from the DEM simulations are illustrated in Figure 8, which presents snapshots of the spatial distributions of incremental contact pressure compared to initial stage and vertical particle velocity around the cone tip. A concentrated zone of elevated contact pressure develops beneath and around the cone during penetration, accompanied by localized particle

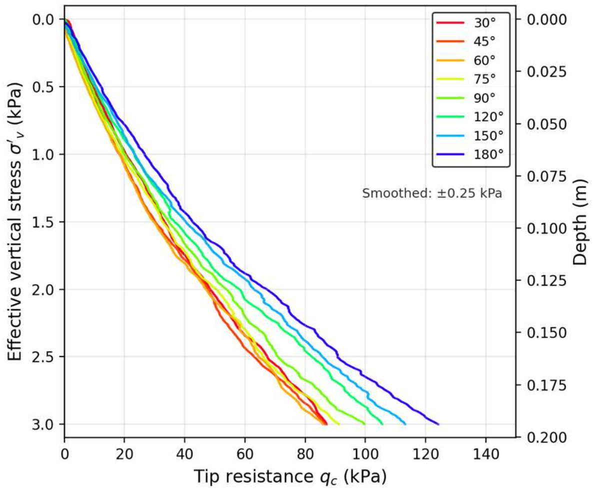

Figure 6 Numerical relationship between q_c and σ'_v evaluated at the cone shoulder (DEM data), after moving-average smoothing (± 0.25 kPa).

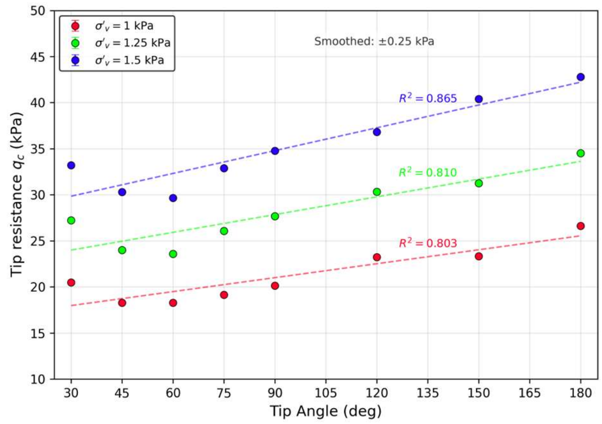

Figure 7 Numerical dependence of q_c on cone tip angle at different σ'_v levels (DEM data)

motion. While the overall structure of this zone is similar for all cone geometries, variations in its intensity and spatial extent are observed among different cone tip angles. The main observations are as follows:

- The contact pressure distribution: Penetration is associated with the development of a concentrated zone of high contact pressure beneath and around the cone. For larger tip angles (e.g., 150° and 180°), this high-pressure zone becomes more intensely localized and laterally extended compared to the slender 30° cone, where the stress is distributed more gradually along the conical surface.
- The particle velocity fields highlight that blunter cones (larger angles) force a more significant volume of soil to move upward and circulate near the shoulder. This interaction leads to the development of a force chain that intensifies particle confinement in the vicinity of the cone. This enhanced confinement under blunter

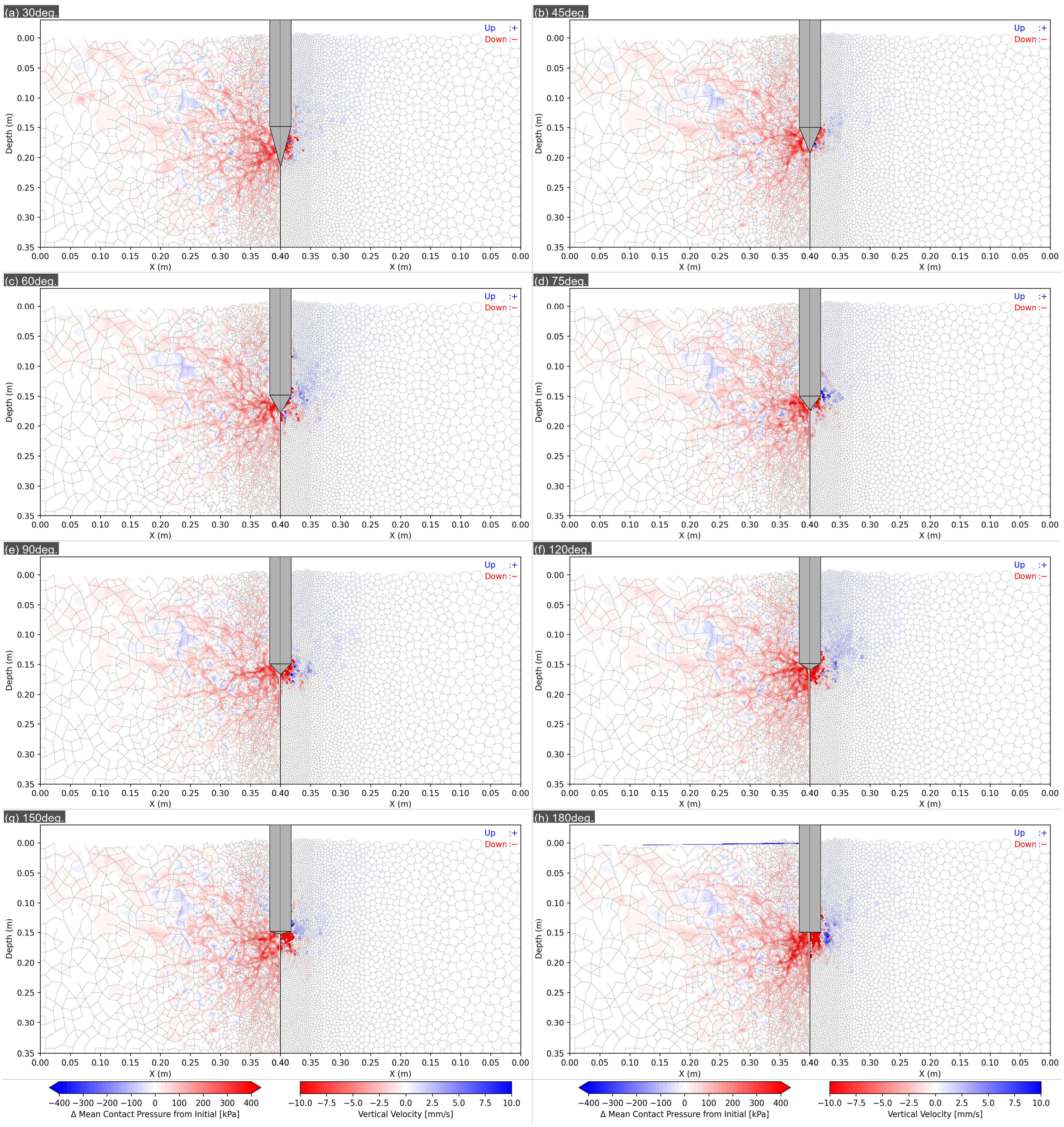

Figure 8 Spatial distribution of incremental mean contact pressure and particle vertical velocity at a penetration depth of approximately 150 mm from DEM simulation.

geometries correlates with the higher q_c values observed.

- The angle-stress synergy: The numerical results reproduce the increase in q_c with increasing cone tip angle at a given effective stress level. This dependency becomes more pronounced at higher stress levels, suggesting that increased confinement amplifies the energy required for the localized particle displacement and force chain rearrangement identified in the shoulder region.

4.3 Discussions

The DEM simulations provide a numerical interpretation of the stress- and geometry-dependent trends observed in the physical model CPT experiments. The numerical results confirm that q_c is governed by both σ'_v level and the cone tip angle. Consistent with the experimental observations, the DEM results show a monotonic increase in q_c with increasing σ'_v for all cone geometries. When σ'_v is evaluated at the cone shoulder depth, the numerical data can be systematically organized across different cone tip angles, demonstrating a clear stress dependency of the simulated q_c. These trends are in good qualitative agreement with the experimental results.

The spatial distributions shown in Figure 8 offer critical micromechanical insights into why these macroscopic trends occur. As the cone tip angle increases, the DEM analysis reveals a distinct transition in the contact pressure distribution and particle kinematics. Overall, the numerical modelling captures the essential features of the experimentally observed dependencies, while clarifying that the shape effect of the cone is primarily driven by the intensity of the localized contact force transmission and the specific volume of mobilized particles around the cone shoulder.

Note that the physical tests used a 12 mm cone to minimize boundary effects, whereas the DEM simulations modeled a standard 35.7 mm cone. Thus, the current comparison remains qualitative, focusing on fundamental mechanisms. Future work will perform DEM simulations with an exact 12 mm cone and incorporate realistic particle shapes for direct quantitative validation.

5 CONCLUSIONS

This study investigated the influence of cone tip angle and the effective vertical stress σ'_v on cone tip resistance q_c through a series of physical model experiments and DEM simulations. The main findings are summarized as follows:

1. Both experimental and numerical results demonstrate that q_c increases monotonically with increasing σ'_v. By evaluating σ'_v at the cone shoulder depth, the stress dependency of q_c can be systematically characterized across different cone geometries.
2. The cone tip angle significantly affects the magnitude of q_c. At a given effective stress level, blunter cones (larger tip angles) yield higher q_c values. This trend is consistently observed in both the laboratory tests and the DEM analysis.
3. The DEM simulations clarify the micromechanical origin of this angle dependency. For larger tip angles, the flat geometry prevents smooth particle flow along the cone surface, forcing a greater volume of soil to exhibit upward motion and strong disturbance around the cone shoulder. This force chain enhances local particle confinement and contact pressure, leading to the observed increase in macroscopic q_c.
4. The numerical results are consistent with the qualitative trends of the physical experiments, confirming that the "shape effect" in CPT is driven by the interaction between cone geometry and the localized stress field.

These insights contribute to a more fundamental understanding of how cone geometry influences soil characterization, providing a basis for interpreting CPT data where non-standard cone geometries might be encountered.

Future studies will introduce realistic particle shapes and exact physical dimensions to the DEM framework to enable rigorous quantitative validation.

ACKNOWLEDGEMENTS

This research was commissioned by the Ports and Harbours Bureau, Ministry of Land, Infrastructure, Transport and Tourism, Japan. The authors gratefully acknowledge this support.

REFERENCES

Ahmadi, M. M. (2009). *Analysis of cone tip resistance in sand*. https://doi.org/10.14288/1.0063502

Ahmadi, M. M., & Karambakhsh, P. (2010, May 1). *K0 determination of Sand Using CPT Calibration Chamber*.

Baligh, M. M. (1985). Strain Path Method. *Journal of Geotechnical Engineering*, *111*(9), 1108–1136. https://doi.org/10.1061/(ASCE)0733-9410(1985)111:9(1108)

Bolton, M. D., Gui, M. W., Garnier, J., Corte, J. F., Bagge, G., Laue, J., & Renzi, R. (1999). Centrifuge cone penetration tests in sand. *Géotechnique*, *49*(4), 543–552. https://doi.org/10.1680/geot.1999.49.4.543

Ciantia, M. O., O'Sullivan, C., & Jardine, R. J. (2019). Pile penetration in crushable soils: Insights from micromechanical modelling. *Proceedings of the XVII European Conference on Soil Mechanics and Geotechnical Engineering*, (Geotechnical Engineering, foundation of the future), 5247–5266. https://doi.org/10.32075/17ECSMGE-2019-1111

Durgunoglu, H. T., & Mitchell, J. K. (1973). *Static penetration resistance of soils* (SSL-SER-14-ISSUE-24). https://ntrs.nasa.gov/citations/19730019713

Iikawa, N., & Katsuragi, H. (2024). *Tip angle dependence for resistive force into dry granular materials at shallow cone penetration* (Version 1). arXiv. https://doi.org/10.48550/ARXIV.2409.14291

Janda, A., & Ooi, J. Y. (2016). DEM modeling of cone penetration and unconfined compression in cohesive solids. *Powder Technology, Particle Modelling with the Discrete Element Method A Success Story of PARDEM (Www.Pardem.Eu)*, *293*, 60–68. https://doi.org/10.1016/j.powtec.2015.05.034

Lei, J., Zhang, N., Arroyo, M., & Oryem Ciantia, M. (2024). Discrete-element based simulation of CPT and

SPT on a volcanic sand. *Computers and Geotechnics*, *170*, 106272. https://doi.org/10.1016/j.compgeo.2024.106272

Mcdowell, G. R., Falagush, O., & Yu, H.-S. (2012). A particle refinement method for simulating DEM of cone penetration testing in granular materials. *Géotechnique Letters*, *2*(3), 141–147. https://doi.org/10.1680/geolett.12.00036

Mindlin, R. D., & Deresiewicz, H. (1953). Elastic Spheres in Contact Under Varying Oblique Forces. *Journal of Applied Mechanics*, *20*(3), 327–344. https://doi.org/10.1115/1.4010702

Nowatzki, E. A., & Karafiath, L. L. (1972). *The Effect of Cone Angle on Penetration Resistance*.

Plimpton, S. (1995). Fast Parallel Algorithms for Short-Range Molecular Dynamics. *Journal of Computational Physics*, *117*(1), 1–19. https://doi.org/10.1006/jcph.1995.1039

Sharif, Y. U., Brown, M. J., Ciantia, M. O., Cerfontaine, B., Davidson, C., Knappett, J., Meijer, G. J., & Ball, J. (2021). Using discrete element method (DEM) to create a cone penetration test (CPT)-based method to estimate the installation requirements of rotary-installed piles in sand. *Canadian Geotechnical Journal*, *58*(7), 919–935. https://doi.org/10.1139/cgj-2020-0017

Yu, H. S., & Mitchell, J. K. (1998). Analysis of Cone Resistance: Review of Methods. *Journal of Geotechnical and Geoenvironmental Engineering*, *124*(2), 140–149. https://doi.org/10.1061/(ASCE)1090-0241(1998)124:2(140)

Zhuang, P.-Z., & Yu, H.-S. (2018). Size Effects in Cone Penetration Tests in Sand. In W. Wu & H.-S. Yu (Eds.), *Proceedings of China-Europe Conference on Geotechnical Engineering* (pp. 283–287). Springer International Publishing. https://doi.org/10.1007/978-3-319-97112-4_64